Hydrodynamic behavior of coarse bioclastic sand under current: A flume experiment.

P. Weill, D. Mouazé & B. Tessier
UMR CNRS 6143 « Morphodynamique Continentale et Côtière », Caen, France

ABSTRACT: Cheniers from the Mont-Saint-Michel Bay (France) are coarse shelly sand ridges migrating on the mudflat up to the salt marshes where they accumulate and merge in a littoral barrier. In a macrotidal setting and low wave forcing, the cheniers are rarely submerged. However, they are found to move up to several meters during coincidence of spring tide and severe storm events. Their morphology, internal structure and processes of migration are thought to be closely related to the hydrodynamic behaviour of the coarse and shelly sediment. This paper focuses on the hydrodynamic behaviour of the sediment: Threshold of motion, velocity profiles and turbulence in the boundary layer above a shell debris bed have been investigated under unidirectional current. A modification of the boundary layer has been identified in the bedload sheet. The flat-shaped bioclastic particles feature low settling velocities and revealed a high resistance to the flow when imbricate in a bed.

1 INTRODUCTION

The southern coast of the Mont-Saint-Michel Bay (Brittany, France) is bordered by a coarse, shelly littoral barrier fringing the edge of the tidal flat. The actual sedimentary filling of the estuary driven by strong asymmetric tidal currents induces a progradation of the salt marshes. The waves, reworking the seafloor of the embayment, sort and concentrate coarse sand, bioclastic debris and whole shells in sheets. Due to the large tidal range (up to 14m at spring tides), these shelly sheets migrate across the tidal flat, evolving on the upper flat in shore parallel elongated structured banks (Bonnot-Courtois et al., 2004). Stratigraphically, the last progradational sediment wedge (i.e. from 2300 BP) of the embayment (the White Dol Marshes) is episodically interrupted by such shell banks anchored in the silty sediment. This configuration is in good agreement with the definition of chenier given by Otvos and Price (1979). If several studies focus on the genesis of cheniers from a stratigraphic or a morphodynamic point of view (Augustinus, 1989), there is very few quantitative flume experiments on the behavior of the shelly material that constitute such bodies.
The aim of this paper is to provide a first step in the understanding of the evolution processes, morphology and internal structure of these coarse littoral barriers by studying the behavior of the bioclastic sediment in a unidirectional current. This experimental study, conducted in a small recirculating flume, belongs to a much larger research project including field works and wave flume experiments. It provides interesting results that allow first quantification of bed roughness and sediment motion threshold.

2 METHODOLOGY

2.1 *Sediment analysis*

Sediment samples collected on the cheniers of the Mont-Saint-Michel bay consist of a mixture of heterometric shell debris and fine siliclastic sand reworked by waves and currents from the tidal flat. Shell debris are plate-shaped, curvated and angular. They offer a large lift surface to the flow. Siliclastic sand is mainly composed of sub rounded quartz grains and heavy minerals. Sediment samples were dried, weighted and sieved in a vibrating column. Grain-size analysis revealed a strong bimodal distribution (Fig. 2). The finest mode is mainly represented by the siliclastic sand and a fine shell ash (including foraminifera).

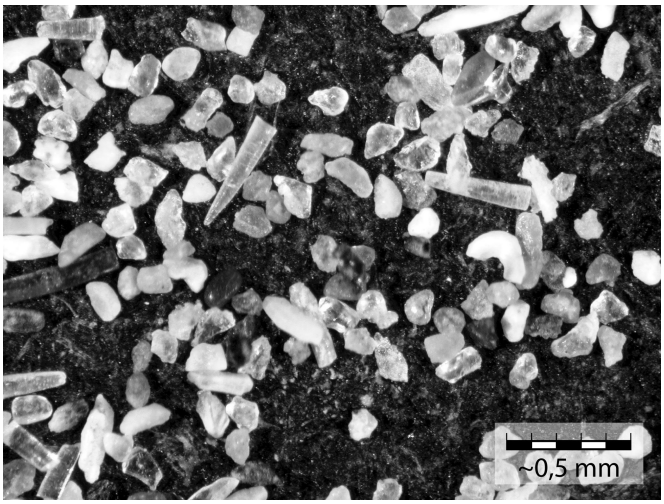

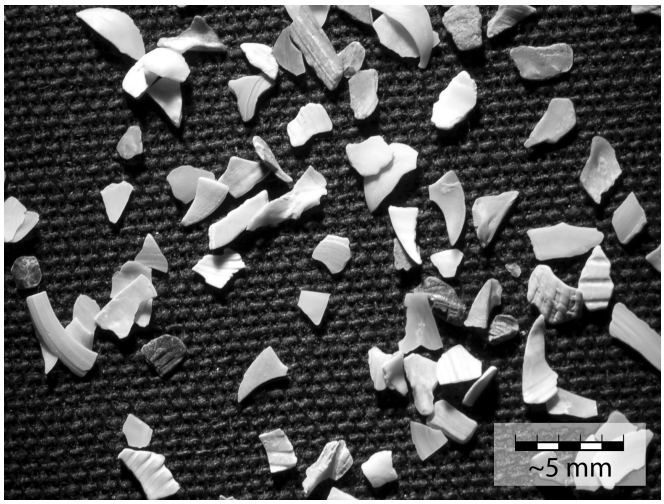

Figure 1. Left: Photograph of the fine siliclastic sand (0.1 - 0.125mm fraction) showing rounded quartz grains and sponge spicules. Right: Photograph of the shelly fraction (1.25 – 3.15 mm); the bioclastic particles are flat, slightly convex and angular. They offer a large lift surface to the flow.

The coarsest mode is exclusively composed of shell fragments. As these two sediment stocks have a very different origin and composition, they are assumed to have a different hydrodynamic behavior. It was thus decided to investigate both the raw sediment (M01) and the two separated modes (coarse: M02, and fine: M03). Sediment characteristics of each sample are summarized in Table 1.

As suggested by Komar and Clemens (1986), the equivalent diameter derived from the settling velocity is more representative of irregular grains shape and hydrodynamic behaviour than the commonly used sieve diameter. In order to obtain a "median equivalent grain size" for each sediment samples, settling velocities of bioclastic particles were measured inside a two meters long sedimentation tube. For each sieve size class obtained via the vibrating column, settling velocities of between 80 and 100 particles were measured using stroboscopic photographs: a bioclast is released from the top of the water column without initial velocity. When its equilibrium velocity is reached, a photograph of the particle is taken with a 2 s exposure time and a 5 Hz stroboscopic lightning. The final image displays 10 successive positions of the particle, separated by a 0.2s time lap. By measuring the distance between each position, the settling velocity can be inferred with a good precision. Velocities are then converted in equivalent diameters using the Gibbs et al. (1971) equation. The results are shown on figure 3. The bigger the sieve size, the more the equivalent diameter differs from the sphere settling velocity (y=x curve). The flat shape gives a large lift surface to the particle which increases the surface drag and reduces its settling velocity.

Table 1. Median grain sieve size and sorting index, equivalent median diameter and sorting index, and density of the three sediment samples.

Sediment samples	D_{50} mm	σ	$D_{50\ settling}$ mm	$\sigma_{settling}$	ρ kg.m^{-3}
M01	0.70	0.48	0.39	0.55	2675.5
M02	0.78	0.42	0.49	0.27	2711.5
M03	0.19	0.08	0.26	0.31	2603.9

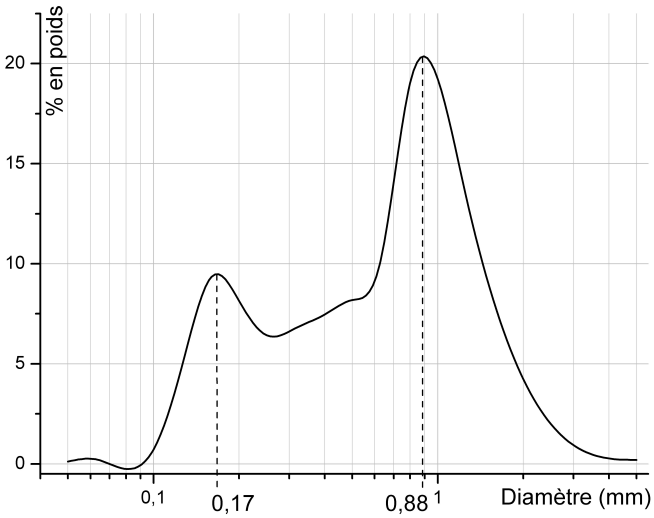

Figure 2. Size distribution of the sediment sampled on a chenier.

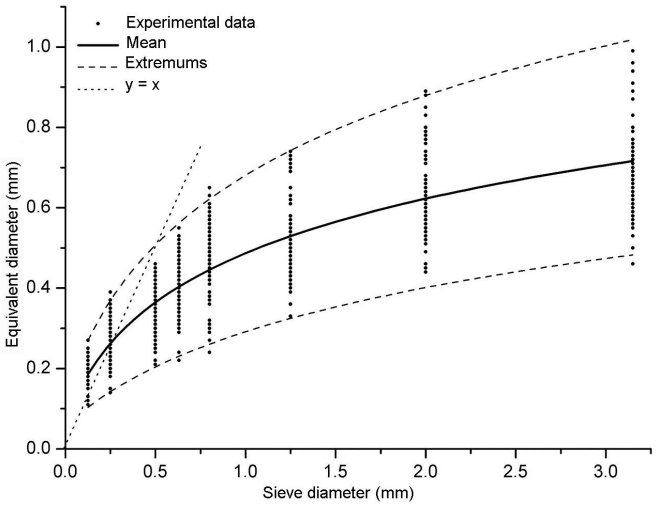

Figure 3. Relation between sieve size and equivalent diameter of bioclastic particles, calculated from the experimental settling velocities using Gibbs equation.

2.2 *Experimental procedure*

Experiments were conducted in a steady-flow, 200 × 10 × 25 cm recirculating flume (c.f. Fig. 4). The discharge is adjusted by a valve and upstream and downstream water gates to create a free surface slope and to control the water depth. An alveolar foam and a honeycomb-like structure are placed at the outflow to ensure a laminar flow.
Sediment sample was distributed between two wedges, and positioned at the center of the flume. The sediment bed is 1 m long and 2.5 cm thick. The water-saturated loose sand is placed in the flume and leveled carefully at the same height as the wedges. It is then slowly flooded, and a current is generated when the desired water depth is reached.

Laser-Doppler Velocimetry (LDV) was used on back scattered mode to characterize the turbulent boundary layer by measuring the velocity and turbulent intensity profiles above the bed. The LDV system operates on the differential Doppler principle. The key component is a pair of crossing laser beams produced by splitting the beam from a single argon-ion laser (Spectra-Physics Series 2000). When the two coherent laser beams intersect at an angle they form an interference fringe pattern. The region where the beams cross is called the measurement volume and here is about 150μm^3. A photo detector receiving the signal records the frequency of the reflected light, from which the velocity of the particle can be determined. Assuming the seeding particles are small and move perfectly with the fluid, the fluid velocity can be inferred.
Here, horizontal and vertical velocities were recorded using respectively a green (514.5 nm) and a blue (488 nm) pair of laser beams.
The LDV system has a small spatial resolution: Vertical profiles were sampled using a step of 0.1 mm in the first millimeter, 1 mm for the first centimeter and 1 cm for the rest of the outer flow. The rate of validated data acquisition is about 60 Hz. The main advantage of this method is that the measuring system is non intrusive, avoiding any disturbance of the flow. The measurement system was positioned one meter (x) downstream of the convergent. It satisfies the Gressner's condition for fully developed flow ($x/(4R)\geq 60$), regarding to the hydraulic radius R of the flume (Nezu and Rudi, 1986). The angle of each pair of beams bed was shifted to 45° related to an horizontal plane, in order to get closer to the channel bed.

The instantaneous horizontal and vertical velocities are filtered at three standard deviations and split into a mean (u,w) and a turbulent velocity (u',w'):

$$u=\bar{u}+u'; \quad w=\bar{w}+w' \tag{1}$$

From this velocity decomposition, we calculate the total shear stress which is the sum of the viscous and the Reynolds (turbulent) stress:

$$\tau_{total}=\underbrace{\mu\frac{\partial u}{\partial z}}_{\tau_{viscous}}-\underbrace{\rho\overline{u'w'}}_{\tau_{turbulent}} \tag{2}$$

The bottom shear or friction velocity is defined by dimensioning τ_{total} as a velocity:

$$u^*=\sqrt{\frac{\tau_{total}}{\rho}} \tag{3}$$

In the viscous sub layer, the classical formulation of the linear evolution of the velocity with the height is considered:

$$\frac{u}{u^*}=\frac{u^*z}{\nu} \tag{4}$$

In the logarithmic layer, several equations are accepted, depending on the flow regime and the parameters to emphasize. Over a smooth bed, Prandlt's law of the wall gives :

$$\frac{u}{u^*}=\frac{1}{\kappa}\ln\left(\frac{u^*z}{\nu}\right)+B \tag{5}$$

where κ is the von Karman constant (≈0.4), and B a constant.

Over a rough bed, we have (Dyer, 1986):

$$\frac{u}{u^*}=\frac{1}{\kappa}\ln\left(\frac{z}{z_0}\right)+C \tag{6}$$

where z_0 is the roughness length and C a constant.

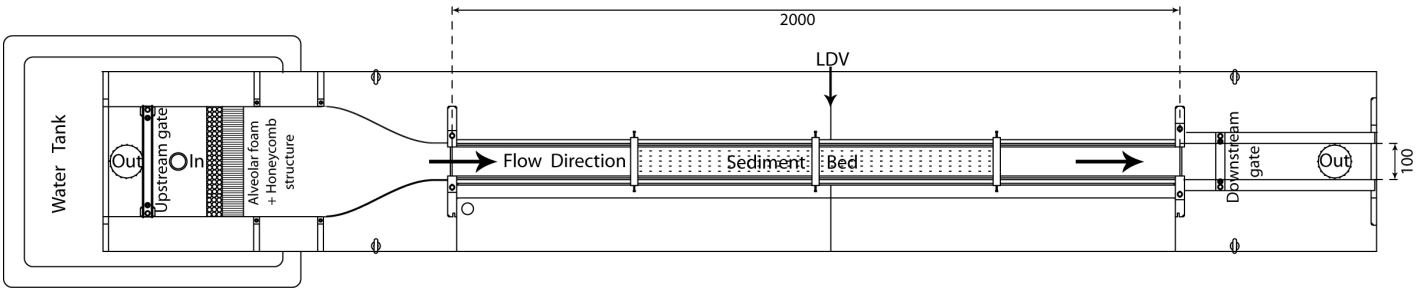

Figure 4. Plan view of the recirculating flume and position of the measurement device (LDV). All dimensions are in millimeters.

Table 2. Experimental parameters. Sporadic and fully developed bedload are indicated by one and two stars respectively. M01: raw - M02: coarse - M03: fine sample

Run	H [cm]	U_{mean} [m/s]	$u^*_{viscous}$ [m/s]	u^*_{log} [m/s]	Re*	z_0 [m]	k_s [m]
			(Eq. 3)	(Eq. 5 or 6)	(Eq. 7)		
M01-D01	6.5	$3.73\ 10^{-2}$	$9.43\ 10^{-4}$	$9.48\ 10^{-3}$	5.59	$2.99\ 10^{-3}$	N/A
M01-D02	6.5	$7.91\ 10^{-2}$	$9.53\ 10^{-4}$	$2.42\ 10^{-2}$	14.28	$2.49\ 10^{-3}$	N/A
M01-D03*	6.5	$1.47\ 10^{-1}$	$1.12\ 10^{-2}$	$1.45\ 10^{-2}$	8.56	$1.60\ 10^{-4}$	$4.55\ 10^{-3}$
M01-D04*	4.5	$2.37\ 10^{-1}$	$2.10\ 10^{-2}$	$2.19\ 10^{-2}$	12.89	$1.30\ 10^{-4}$	$3.78\ 10^{-3}$
M01-D05**	4.8	$3.55\ 10^{-1}$	$2.22\ 10^{-2}$	$1.75\ 10^{-2}$	13.11	$1.00\ 10^{-4}$	$2.88\ 10^{-3}$
M02-D01	6.5	$3.06\ 10^{-2}$	$1.32\ 10^{-3}$	$7.69\ 10^{-3}$	7.69	$4.36\ 10^{-3}$	N/A
M02-D02	6.5	$8.76\ 10^{-2}$	$5.60\ 10^{-3}$	$1.29\ 10^{-2}$	12.87	$7.30\ 10^{-4}$	N/A
M02-D03*	6.5	$1.83\ 10^{-1}$	$6.59\ 10^{-3}$	$1.34\ 10^{-2}$	13.44	$8.00\ 10^{-5}$	$1.92\ 10^{-3}$
M02-D04*	4.5	$2.82\ 10^{-1}$	$1.65\ 10^{-2}$	$2.06\ 10^{-2}$	21.73	$7.80\ 10^{-5}$	$2.16\ 10^{-3}$
M02-D06**	4.0	$3.44\ 10^{-1}$	$2.58\ 10^{-2}$	$2.30\ 10^{-2}$	23.00	$8.25\ 10^{-5}$	$2.39\ 10^{-3}$
M03-D01	6.5	$5.26\ 10^{-2}$	$2.38\ 10^{-3}$	$9.46\ 10^{-3}$	2.27	$1.96\ 10^{-3}$	N/A
M03-D02	6.5	$1.28\ 10^{-1}$	$1.78\ 10^{-3}$	$2.03\ 10^{-2}$	4.86	$7.50\ 10^{-4}$	N/A
M03-D03**	6.5	$2.02\ 10^{-1}$	$1.50\ 10^{-2}$	$1.15\ 10^{-2}$	3.61	$5.30\ 10^{-4}$	$1.38\ 10^{-3}$

The boundary Reynolds number which characterizes the flow regime in the boundary layer can be defined as followed, with D the median grain diameter:

$$Re^* = \frac{\rho D u^*}{\mu} \quad (7)$$

If $Re^* \leq 5$, the flow is said "hydraulically smooth". The element's roughness is smaller than the viscous sub layer and it doesn't affect the flow. If $Re^* \geq 65$, the flow is "hydraulically rough". The roughness elements protrude beyond the viscous sub layer producing a wake behind each grain. Viscosity has less influence on both the velocity distribution and the overall drag on the surface. If $5 \leq Re^* \leq 65$, we have a transitional state; the roughness elements are about the same size as the viscous sub layer. The vertical velocity distribution is more complex and still poorly predicted (LeRoux, 2004).

3 RESULTS AND DISCUSSION

A number of 13 experiments were carried out over the three sediment samples under various water discharge rates. Initially low, the fluid velocity was increased incrementally until a general bed load is observed. Between each step, a velocity profile was measured through the whole water column. The experimental parameters are summarized in table 2.

3.1 *Velocity and stress profiles*

For each velocity profile, the experimental data are fitted on the theoretical curves: The bottom shear velocity u* has been estimated both from Eq. 4 and Eq. 6, and compared, as suggested by Afzalimehr and Anctil (2001). The values are reported in Table 2. As the discharge rate is increased, the bottom shear velocity increases, the boundary Reynolds number increases, and the roughness length decreases. However, there is some differences for the calculated bottom shear velocities between the two methods ($u^*_{viscous}$ and u^*_{log} in Table 2). If the values are of the same order of magnitude for medium discharge rates (M01-DO3 and D04, M02-D04, M03-D02), the ones extrapolated from the bottom shear stress are significantly underestimated compared to the log layer fits for low discharge rates (M01-D01 and D02, M02-D01 and D02, M03-D01), and a bit greater for the maximum velocities.

In figure 5 are plotted three representative velocity profiles above the raw sediment bed (M01-D01, M01-D03 and M01-D05). They point out the evolution of the boundary layer as the velocity is increasing. The very high resolution of the LDV allow us to observe the thinning down of the viscous sub-layer.

For all of the sediment samples (raw - M01, coarse - M02 and fine mode - M03), there is a striking change in the boundary layer as the bedload become generalized (Fig.5, M01 D05). We can identify a logarithmic growth of the velocity in the bedload sheet (log layer 1), just below the classical log layer (log layer 2). The velocity gradient of the log layer 2 is lower than in the log layer 1. This is a significant change of the trend with what can be seen below the threshold of motion: When the sediment is still, the "no velocity condition" at the bottom implies a large shear stress in the water column and so a large velocity gradient in the log layer. When the bed-load is initiated, the log layer doesn't “see” a fixed bed as previously, but a moving layer of sediment (log layer 1). The shear stress is slightly released in the water column and the velocity gradient in the log layer 2 is lower. Further investigations are required to confirm and explain this phenomenon with more details.

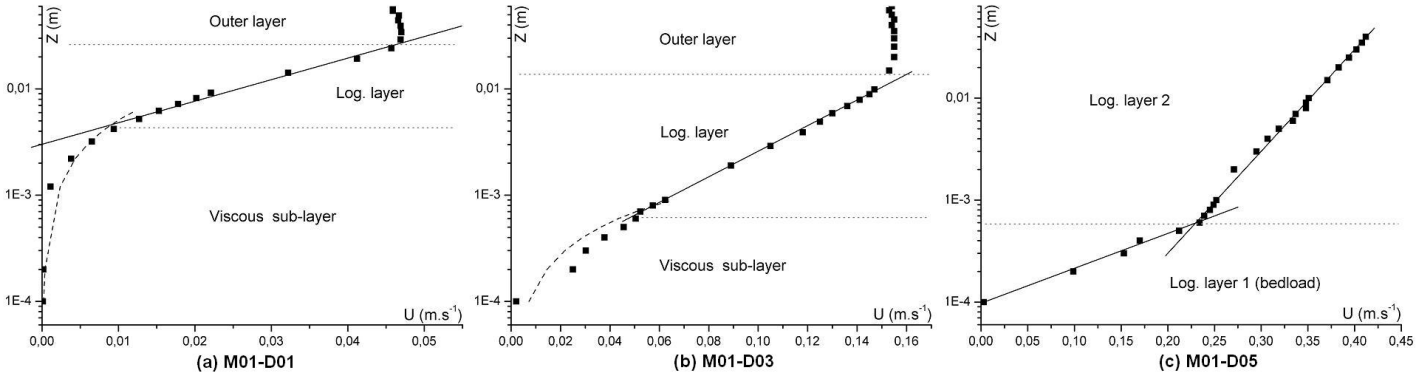

Figure 5. Velocity profiles across the water column for the raw sediment (M01) at three discharge rates, below (a), at (b) and above (c) the critical shear stress (note the change of scale on the abscissa).

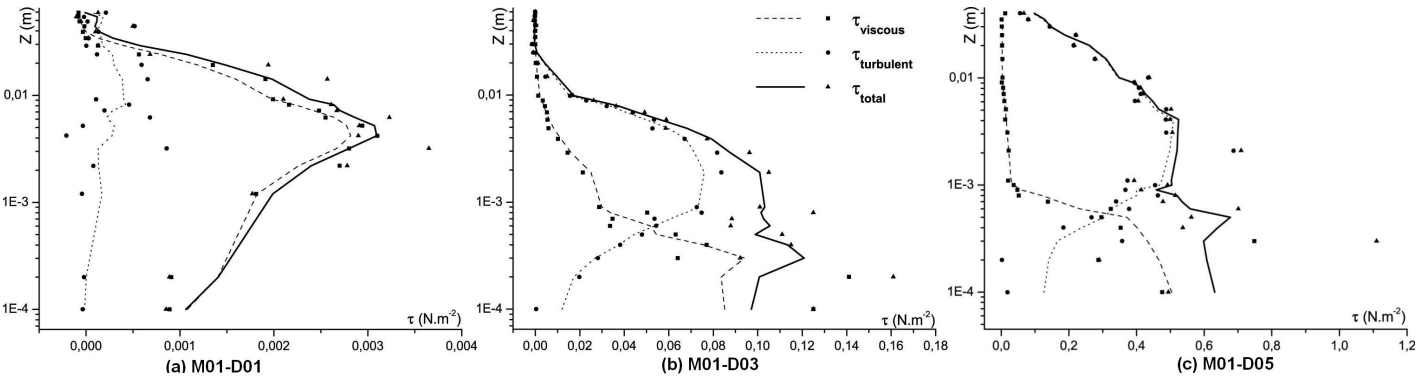

Figure 6. Stress profiles across the water column for the raw sediment (M01) at three discharge rates, below, at and above the critical shear stress (note the change of scale on the abscissa).

Figure 6 shows the viscous, turbulent and total stress profiles (c.f. Eq.2) corresponding to the three above-mentioned velocity profiles.

The first one (M01-D01) shows clearly a laminar flow. The turbulent stress is very small on the whole water column, and the viscous stress dominates. With an increased discharge rate (M01-D03 and D05), two distinct regions appear: Near the bed in the first half millimeter, the flow is almost laminar with a low turbulent activity. When general bedload is observed (M01-D05), the turbulent stress represent about one fifth of the viscous stress. This layer couldn't be properly qualified as a viscous sub-layer, which is not as clear as for M01-D01, but there is a clear transition with the upper part where the eddies activity is fully developed.

This transition region (between 0.5 and 1 mm above the bed), features the maximum of total stress in the water column.

3.2 *Roughness of a shell debris bed*

The calculated Reynolds roughness numbers (Re_*) show values ranging from 2 to 5 for the fine sediment sample, and from 5 to 25 for the raw and coarse samples. According to the classification of hydraulic regime, the flow is smooth for the finest sediment, and transitional for the two coarsest. It means that, despite the large sieve diameters of the shell debris, their plate-like shape allows the bed to organize itself on a very flat way, minimizing the grain protrusion in the flow and the development of an intense turbulent activity. This observation emphasizes the importance to define properly the element roughness height k for such a specific sediment. This parameter used to describe the boundary layer profile is often taken as the median grain diameter, and is obviously smaller in the case of a shell debris bed. The very precise sampling of the boundary layer allows a direct measurement of the roughness length of the bed (z_0) from the velocity profiles. This parameter is given by the extrapolation of the log layer to u = 0, and gives an indication of the roughness height. z_0 is found to decrease with increasing current velocity, which is consistent with the transitional flow regime where (Van Rijn, 1993) :

$$z_0 = 0.11\frac{\nu}{u^*} + 0.033 k_s \qquad (8)$$

with k_s the Nikuradse equivalent roughness. The calculated values of k_s are reported in Table 2. For the lower discharge rate, the flow is smooth and this roughness length looses its meaning (N/A in Table 2). The values are a bit scattered but are a good indication of the Nikuradse roughness length for a shell debris bed.

3.3 *Sediment motion threshold*

The threshold of movement of a sediment is the key parameter to understand and interpret the environmental conditions of building or transformation

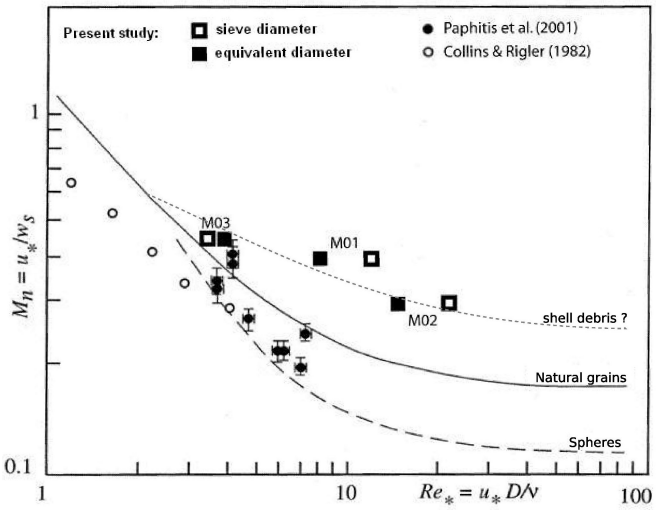

Figure 7. Threshold of motion for the three sediment samples expressed in term of mobility number, plotted over the synthetic diagram of Paphitis et al. (2001).

of a sedimentary body (Kench & McLean, 1996).

The Shields parameter (Shields, 1936) is widely used as a dimensionless threshold. However, itsmain limitation is that it doesn't take into consideration the shape of the particles. Komar & Clements (1986) defined a mobility number that takes into account the critical shear velocity and the settling velocity of the sediment:

$$M_n = \frac{u^*}{w_s} = \sqrt{\frac{\tau_{cr}}{\rho}} \cdot \frac{1}{w_s} \quad (9)$$

Using this parameter, the influence of the particles shapes, which was shown to be especially important for shell debris, is introduced via the settling velocity.

For each of the three sediment samples, the critical shear stress was calculated from the velocity profiles, and divided by the median settling velocity. The results are reported in figure 7, and compared to other experimental data obtained with spheres and natural grains (Paphitis et al., 2001). The finest fraction, mainly composed of siliclastic sand, is in good agreement with the mobility number of natural siliclastic grains. For the bioclastic fractions, it is clear that the initiation of motion requires higher velocities than for regular natural grains of the same size: when organized in a bed, the shell debris with their flat shape, offer a very small surface to the flow, compared to their sizes. It results a higher resistance to the flow.
The sediment shows also a high capacity of bed armoring. The threshold of motion was found to increase with an increased pre-threshold velocity exposure time: as an incipient motion is observed, the more instable grains relocate themselves into a more sheltered position, and quickly no more movement is observed. The discharge rate needs to be increased to reach an effective bedload. This observation has been made by Paphitis and Collins (2005).

We can also notice that the raw sediment sample features a higher threshold than the coarse fraction. This can be easily explained by the fact that the fine sand contained in the raw fraction stabilizes the bed and the coarse debris between each other. By filling the pores, the fine sand cements the bed.

4 CONCLUSION

Results presented here are a first step in the study and need to be considered with caution. Further investigation needs to be done with better sorted shell debris samples.
This hydrodynamic study revealed the complex behaviour of the bioclastic material that composes shelly cheniers. The sediment is polygenetic and heterogeneous. If the shape of the particles confers a large lift surface and a small settling velocity when in suspension, the sediment shows a high resistance to the flow when structured in a bed.

The LDV system allows a very good sampling in the boundary layer. All the relevant parameters characterizing its structure can be directly calculated. This is useful in the case of a bioclastic sediment where the commonly used estimations for rounded quartz grains couldn't be applied. However, more tests need to be done in order to refine the results. We plan new experiments over glued sediment bed to compare with a mobile bed in order to explain the feedback of bedload on the boundary layer structure. Minor adjustments will be done on the flume to increase the potential of discharge rate.

The dual behaviour of the shell debris might be a key to understand how does this coarse material accumulate across the tidal flat, and concentrate to form a whole structured sedimentary body. One can expect major differences of transport of these coarse particles when isolated on a smooth bed (the mixed mud and sand flat) or moving over a rough bed made of other shell debris. The large lift surface of the shell debris allow them to be easily sorted from the fine siliclastic sand, and transported across the tidal flat by swash and current processes as the tide rise up. When reaching the level of maximum flooding of the most frequent high tides, theses debris accumulate in sheet, and their behaviour is suspected to change. They form coarse swash bars, with high porosity properties. Bed armouring become a major feature, allowing sand layers to be accreted, with different thickness, sorting and composition depending of the hydrodynamic conditions.

This first quantification of the hydrodynamic behaviour of coarse bioclastic sand will be integrated and will help to understand more complex processes which will be modelled in a flume experiment including wave activity and tidal fluctuations.

AKNOWLEDGEMENT

This work is carried out within the framework of a PhD funded by the *Conseil Régional de Basse-Normandie*.

REFERENCES

Afzalimehr, H. and Anctil, F. (2001) Friction velocity associated to a non-uniform flow and an intermediate scale roughness. Journal of Hydraulic Research, 39-2, 181-186.

Augustinus, P. (1989) Cheniers and chenier plains: a general introduction. Marine Geology, 90, 219-229.

Bonnot-Courtois, C., Fournier, J. and Dréau, A. (2004) Recent morphodynamics of shell banks in the western part of Mont-Saint-Michel Bay (France). Géomorphologie: relief, processus, environnement, 1, 65-80.

Dyer, K. (1986) Coastal and estuarine sediment dynamics: John Wiley & Sons, 342 pp.

Gibbs, R.; Matthews, M. & Link, D. (1971) The relationship between sphere size and settling velocity, Journal of Sedimentary Petrology 41-1, 7-18.

Kench, P. and McLean, R. (1996) Hydraulic characteristics of bioclastic deposits: new possibilities for environmental interpretation using settling velocity fractions. Sedimentology, 43, 561-570

Komar, P. and Clemens, K. (1986) The relationship between a grain's settling velocity and threshold of motion under unidirectional currents. Journal of Sedimentary Petrology, 56-2, 258-266.

LeRoux, J. (2004) An integrated law of the wall for hydrodynamically transitional flow over plane beds. Sedimentary Geology, 163, 311-321.

Nezu, I. and Rodi, W. (1986) Open-channel flow measurements with a Laser Doppler Anemometer. Journal of Hydraulic Engineering 112-5, 335-355

Otvos, E. and Price, W. (1979) Problems of chenier genesis and terminology - An overview. Marine Geology, 31, 51-263.

Paphitis, D.; Velegrakis, A.; Collins, M. and Muirhead, A. (2001), Laboratory investigations into the threshold of movementof natural sand-sized sediments under unidirectional,oscillatory and combined fow', Sedimentology 48, 645-659.

Paphitis, D.; Collins, M.; Nash, L. and Wallbridge, S. (2002), Settling velocities and entrainment thresholds of biogenic sands(shell fragments) under unidirectional flow, Sedimentology 49, 211-225.

Paphitis, D. and Collins, M. (2005) Sand grain threshold in relation to bed "stress history": an experimental study. Sedimentology, 52, 827-838.

Shields, A. (1936) Application of similarity principles and turbulence research to bed-load movement. Translated from "Anwendung der Aehnlichkeitsmechanik un der Turbulenzforschung auf die Geschiebebewegung" by W.P. Ott and J.C. van Uchelen, California Institute of Technology

Van Rijn, L. (1993) Principles of sediment transport in rivers, estuaries and coastal seas: Aqua Publication